 CMES, vol.23, no.3, pp.187-207, 2008

Improving Volume Element Methods by Meshless Radial Basis Function Techniques

P. Orsini[1], H. Power[1,2] and H. Morvan[1]

Abstract: In this work, we present a modified Control Volume (CV) method that uses a Radial Basis Function (RBF) interpolation to improve the prediction of the flux accuracy at the faces of the CV. The method proposed differs from classical CV methods in the way that the flux at the cell surfaces is computed. A local RBF interpolation of the field variable is performed at the centres of the cell being integrated and its neighbours. This interpolation is then used to reconstruct the solution and its gradient in the integration points which support the flux computation. In addition, it is required that such interpolation satisfies the governing equation in a certain number of points placed around the cell centres. In this way, the local interpolations become equivalent to local boundary-value problems. To find the solution to the local problems, we have tested both the unsymmetric (Kansa's method) and symmetric (Hermitian method) RBF approaches. The proposed CV approach will be referred to as the CV-RBF method and validated here in a series of one- and three-dimensional test cases.

1 Introduction

The CV unstructured mesh approach has been widely used in the last twenty years due to the flexibility that the approach offers in the modelling of problems which features complex geometry. However when unstructured meshes are employed instead of structured ones, both cell stencil selection and flux computation become more difficult. Although significant works have been carried out in this field, methods that aim to high order convergence solution with unstructured meshes are still a subject of active research.

In the literature two different approaches are reported when unstructured control volume schemes are considered: Cell-centred and vertex-centred schemes. The second scheme is usually called the Control Volume Finite Element (CV-FEM) scheme. In the cell-centred configuration the CVs used to integrate the governing equation are the elements of the mesh which discretises the problem, and pertinent information concerning the system variables are stored at the centre of these elements. The main ideas behind this scheme, widely used in computational fluid dynamic (CFD), are reported in Versteeg, and Malalasekera (2007); for some practical applications see also Date (2005). In the vertex-centred scheme, system variable information is stored at the vertices of the mesh elements, and the CVs are constructed around these vertices. The field variable within each element is defined in terms of the element nodal values using FE shape functions (linear or quadratic polynomial), and the corresponding gradient is obtained by differentiation of the same shape functions. Since the first publication by Baliga and Patankar (1980) the CV-FEM has been successfully used as a numerical tool in a wide range of application (for more details see Rousse (2000); Liu et al. (2002); Ben Salah et al. (2005); Grissa et al. (2007)).

Regardless of the type of scheme implemented, the accuracy of the CV method discretisation is strongly dependent on the flux approximation which is adopted. This is usually computed considering two contributions; the convective flux and the diffusive flux. Generally each of this term requires a different method of approximation which suits its physical nature. In the vertex-

[1] The University of Nottingham, School of Mechanical, Materials and Manufacturing Engineering, Nottingham, NG7 2RD, United Kingdom

[2] Corresponding author. henry.power@nottingham.ac.uk

centred schemes, the gradient at the CV faces found in the diffusive flux is obtained by differentiation of the shape functions. A different strategy is reported in literature for cell-centred CV methods. In this case the diffusive flux is usually decomposed in terms of appropriately chosen orthonormal vectors Versteeg and Malalasekera (2007). In two-dimensional (2D) problems, the scheme takes account of two different contributions to compute the gradient vector of the field variable at the cell faces: The normal and tangential components. The normal component is finally expressed in terms of two gradient projections: Along the line which joins the two cell centres and along the cell face tangential direction. The first term is obtained by a central finite difference (FD) formula, which is of second order of accuracy only when the adjoining control volumes are of equal length in the normal direction. The second term, the tangential component, is still computed with a second order central FD formula which is function of the cell face end points. As in the cell-centred scheme the values of the function at the face end points are generally unknown, these values are usually obtained by simple averaging over neighbouring cell centres. The evaluation of the gradient using the approach explained above brings a computational error which increases with skewness and the degradation of the element aspect ratio. To avoid this discretization error, Turner and Ferguson (1995) proposed the use of a four-node formula, instead of a two-node one. This approach captures both the normal and tangential components of the gradient vector and consequently reduces the error associated with the domain discretization. Different algorithms are used to compute the convective part of the flux, which requires the evaluation of the variable function at the faces of the control volume. Usually upwind algorithms are used for this purpose in either the cell-centred and vertex-centred schemes. A comprehensive review of the available upwind algorithms is reported in Versteeg and Malalasekera (2007).

In the attempt of increasing the accuracy of unstructured CV schemes, other new ideas regarding the flux reconstruction have been proposed in the last few years. Abgrall (1994) revisited the possibility of performing the flux reconstruction in triangular meshes through the use of local two-dimensional polynomial functions. The same idea has been extended to three-dimensional problems in the weighted essentially non-oscillatory (WENO) CV scheme presented by Dumbser and Kaser (2007). Large attention has also been given to the least squares function reconstruction technique (LSRT). This technique has been used in the computation of flux corrective terms (see Jayantha and Turner (2003), (2005)) to increase the spatial accuracy of CV schemes, and also, in a more direct approach, in the reconstruction of the fluxes at the cell faces of the control volume (see Ollivier-Gooch and Van Altena (2002)). Other researchers proposed the Gauss-Green gradient reconstruction technique (GGRT), which has been used in combination with the LSRT to compute the gradients at the cell faces of the CV (see Truscott and Turner (2004) and Manzini and Putti (2007)).

One possible alternative to improve the accuracy of the evaluation of the diffusive flux is the use of radial basis functions (RBF). In the literature, the RBF interpolation method is considered as an optimal numerical technique for interpolating multidimensional scattered data. Although most work done so far on RBF relates to scattered data approximation and, in general, to interpolation theory, there has recently been an increased interest in the use of RBF as the base of meshless collocation approaches for solving partial differential equations (PDEs) (see Kansa and Hon (2000), unsymmetric approach, and Jumarhon et al. (2000), symmetric approach). While the global formulation of these techniques become unpractical when the number of collocation points is relative large, typically of the order of few thousands, their local implementation can be explored for the improvement of classical numerical methods.

The idea of introducing RBF interpolation to improve the accuracy of a classical numerical scheme has been recently employed by Wright and Fornberg (2006). In this work the authors utilize a Hermitian RBF interpolation to remove the symmetry constraint required to achieve high

order approximation in the FD scheme. The use of RBF interpolation to improve the Boundary Element Method (BEM) has been implemented amount others by Sladek et al. (2005), using a local integral equation formulation, while May-Duy et al. (2006) used a global formulation. On the other hand, Nguyen-Van et al. (2007) incorporates the strain smoothing method for mesh-free conforming nodal integration into the Finite Element Method (FEM). In the context of the CV unstructured mesh approach, Moroney and Turner (2006) (2007), improved Liu et al. (2002) CV approach which uses FE polynomial shape functions, for 2D and 3D problems respectively. Their approach relies on a local RBF interpolation of the field variable, where the CV centres of the considered stencil act as trail points. In particular, Moroney and Tuner consider the ability of their CV-RBF scheme to achieve high accuracy on relatively coarse meshes due to the high accuracy of the RBF interpolation to evaluate derivatives (for more details see Madych (1992) and Fornberg and Flyer (2005)) and thus guaranty a high order approximation of the diffusive flux.

Following Moroney and Turner (2006), (2007), we propose in this article to use a RBF interpolation to improve the accuracy of classical CV schemes. The method introduced here is based on a local RBF interpolation of the field variable at the control volume cell centres, as in the case of Moroney and Turner CV-RBF approach. Besides, in our approach, it is also required that the local interpolation satisfies the governing equation at a set of auxiliary interpolation points and the boundary conditions at the boundary points contained in the local interpolation systems. To guarantee that the interpolation function locally satisfies the governing equation and boundary conditions at boundary points (where present in the local interpolation systems), both the unsymmetric and symmetric RBF meshless approaches are used and their results compared.

In our approach, the solved local systems using the RBF strong form formulation are combined with the CV weak form to solve the global problem. In this way, we use the best features of the two approaches, avoiding the ill-conditioning issues of the global RBF meshless approach for large number of trial and collocation points. Besides, the use of localised RBF for reconstruction step in CV resolves the ill-conditioning issues encountered in Abgrall (1994) and Dumbser and Kaser (2007) for the computation of the polynomial coefficients. In fact, choosing the RBF type appropriately and limiting the number of collocation points used lead to an interpolation that is well posed in all dimensions.

Having an interpolation that satisfies locally the physical operator provides an implicit upwind formulation. Finally, the method proposed here is more flexible than classical CV formulations because the boundary conditions are directly imposed in the interpolation approach, without the need for artificial schemes (e.g. utilising dummy cells).

2. RBF interpolation

In recent years the theory of radial basis functions has undergone intensive research and enjoyed considerable success as a technique for interpolating multivariable data and functions. A radial basis function $\Psi\left(\left\|x-\xi_j\right\|\right)$ depends upon the separation distances of a subset of trial centres $\{\xi_j \in \Re^n;\ j=1,2,\ldots,N\}$ and a field point x. Due to the RBF spherical symmetry around the centres ξ_j (trial points), they are called radial. The distances $\left\|x-\xi_j\right\|$, $j=1,2,\ldots,N$, are usually taken to be the Euclidean metric. The set of field points where the function is evaluated in the interpolation are known as test or collocation points. In RBF interpolation it is usual to select the trial and test points as the same set of points; however this is not necessary in principle.

The most popular RBFs are listed in table 1 below.

The Gaussian and the inverse multiquadric, i.e. $m<0$ in the generalized multiquadric function, are positive definite functions. The thin-plate splines (TPS) and the multiquadric, i.e. $m>0$, are conditionally positive definite functions of order m, which require the addition of a polynomial term of order $m-1$ along with an homogeneous constraint condition (see equation (3) below) in order to obtain an invertible interpolation matrix. The multiquadric functions with values of $m=1$

Table 1: Table of most popular Radial Basis Functions.

Radial basis functions (RBFs)		
Generalized Thin Spline	Generalized Multiquadric	Gaussian
$r^{2m-2}\log r$	$\left(r^2+c^2\right)^{m/2}$	$\exp\left(-r/c\right)$
where m is an integer and $r=\left\|x-\xi_j\right\|$.		

and $c=0$ are often referred to as conical functions and, with $m=3$ and $c=0$, as Duchon cubic.

Even though TPS have been considered optimal in interpolating multivariate functions, they do only converge linearly, (see Powell (1994)). On the other hand, the multiquadratic (MQ) functions converge instead exponentially as shown by Madych and Nelson (1990). However, the MQ functions contain a free parameter, c, often referred to as the shape parameter, when c is small the resulting interpolating surface is pulled tightly to the data points, forming cone-like basis functions and as c increases the peak of the cone gradually flattens. It is worth noticing that the set up of this parameter is not trivial and still a matter of intensive research (see Wright and Fornberg (2006)).

In a typical interpolation problem, we have N pairs of data points $\{(x_i,U(x_i))_{i=1,2,\ldots,N}\}$, which are assumed to be samples of the unknown function U that is to be interpolated by the function u as

$$u(x)=\sum_{j=1}^{N}\alpha_j\Psi\left(\left\|x-\xi_j\right\|\right)+\sum_{j=1}^{NP}\alpha_{j+N}P_{m-1}^{j}(x), \qquad x\in\Re^n \quad (1)$$

in the sense that

$$U\left(x_i\right)=\sum_{j=1}^{N}\alpha_j\Psi\left(\left\|x_i-\xi_j\right\|\right)+\sum_{j=1}^{NP}\alpha_{j+N}P_{m-1}^{j}\left(x_i\right) \quad (2)$$

along with the constraint condition

$$\sum_{j=1}^{N}\alpha_jP_{m-1}^{k}\left(x_j\right)=0, \quad k=1,\ldots,NP \quad (3)$$

Here α_j, with $j=1,\ldots,N,N+1,\ldots,N+NP$, are real coefficients to be found from the interpolation, Ψ is a radial basis function and NP the total number of terms in the polynomial (determined by the polynomial order and the number of spatial dimensions). In order to retain a simple notation we will refer to the polynomial terms which appears in the second term of the right hand side of (2) as P_{m-1}.

The matrix formulation of the above interpolation problem can be written as $A\alpha=B$ with

$$A=\begin{pmatrix}\Psi & P_{m-1}\\ P_{m-1}^{T} & 0\end{pmatrix}, \quad B^T=(U,0) \quad (4)$$

Micchelli (1986) proved that for a case when the test points are all distinct, the matrix resulting from the above radial basis function interpolation is always non singular. Although a matrix such as A is always invertible in theory, i.e. well posed, numerical experiments show that the condition numbers of the matrix obtained with the use of RBF like Gaussian or multiquadric are extremely large when compared with those resulting from the generalized thin-plate splines with low values of m (see Schaback (1995)). Similar issue regarding the condition number to those encountered with the use of the Gaussian or multiquadric functions are found when using the generalized thin-plate splines function with large values of m.

Consider a boundary value problem defined by

$$L[u]=f(x) \text{ on } \Omega \quad (5)$$

$$B[u]=g(x) \text{ on } \partial\Omega \quad (6)$$

where the operators L and B are linear partial differential operators on the domain Ω and at the contour $\partial\Omega$ respectively.

An unsymmetric RBF collocation method, as is the case of the Kansa's method, represents the solution of the above boundary value problem by the interpolation (1). In the collocation scheme of the Kansa's method, the set of N test points are distributed into a set of n boundary points, where the

boundary condition (6) is imposed, and $N-n$ interior points, where the governing equation (5) is required to be satisfied. The trial points are usually chosen to be the same set of test points.

The above expansion for u leads to a collocation matrix A of the form:

$$A = \begin{pmatrix} B_x[\Psi] & B_x[P_{m-1}] \\ L_x[\Psi] & L_x[P_{m-1}] \\ P_{m-1}^T & 0 \end{pmatrix} \tag{7}$$

which is fully populated and non-symmetric.

The unsymmetric approach has been applied to a wide range of problems with great success (see for example Hon and Mao (1998); Fedoseyev et al. (2002); Young et al. (2005) and Wen and Hon (2007)). However, no existence of solution and convergence analysis are available in the literature and it has been reported that, in some cases, the resulting matrices were extremely ill-conditioned and even singular for some distribution of the nodal points (see Dubal et al. (1993)). In those cases where the obtained matrix is singular, it is possible that a small perturbation of the functional centre locations or the value of the shape parameter can result in a non-singular matrix Brown (2005). More recently, Ling et al. (2006) showed asymptotically the feasibility of a generalized variant of the Kansa's method by using separated trial and test spaces. Under this condition, for a sufficiently dense set of N linearly independent continuous trial functions and a set of M test points, which locations are chosen to minimise the residual, the resulting interpolation matrix has full rank N. Then by properly choosing trial centres the resulting Kansa's collocation matrix can be non-singular.

Fasshauer (1997) suggested an alternative approach to the unsymmetric method based on the Hermite interpolation property of the radial basis functions, which states that the RBF not only are able to interpolate a given function but also its derivatives. The convergence proof for RBF Hermite-Brikhoff interpolation was given by Wu (1992) who also proved the convergence of this approach when solving PDEs (see Wu (1998) and Franke and Schaback (1998)). Another advantage of the Hermite based approach is that the matrix resulting from the scheme is symmetric, as opposed to the completely unstructured matrix of the same size resulting from the unsymmetric method.

In the symmetric method, the solution u of the above boundary value problem is defined by

$$u(x) = \sum_{j=1}^{n} \alpha_j B_\xi \Psi\left(\left\|x-\xi_j\right\|\right) + \sum_{j=n+1}^{N} \alpha_j L_\xi \Psi\left(\left\|x-\xi_j\right\|\right) + \sum_{j=1}^{NP} \alpha_{j+N} P_{m-1}^j(x) \tag{8}$$

with n as the number of nodes on the boundary, $\partial\Omega$, and $N-n$ the number of internal nodes. In the above expression L_ξ and B_ξ are the differential operators used in (5) and (6) but acting on Ψ viewed as a function of the second argument ξ. This expansion for u leads to a symmetric collocation matrix A, which is of the form

$$A = \begin{pmatrix} B_x B_\xi[\Psi] & B_x L_\xi[\Psi] & B_x P_{m-1} \\ L_x B_\xi[\Psi] & L_x L_\xi[\Psi] & L_x P_{m-1} \\ B_x P_{m-1}^T & L_x P_{m-1}^T & 0 \end{pmatrix} \tag{9}$$

The matrix (9) is of the same type as the scattered Hermite interpolation matrices and thus non-singular provided that no two collocation points sharing operators that are linearly dependent are placed in the same location. For further details on the application of the above RBF Hermitian collocation approach (see La Rocca et al. (2005)).

From a series of simple steady state numerical examples, Fasshauer (1997) concluded that the Hermitian method performs slightly better than Kansa's method in most circumstances. More recently Power and Barraco (2002) found that the unsymmetric method faced some difficulties solving convection-diffusion problems at high Péclet number, which do not occur when using the Hermitian approach.

The computational costs of both the symmetric and unsymmetric methods are very high due to the use of global interpolation functions in the representation of the problem solution, resulting in fully populated coefficient matrices. Besides, the

matrices obtained tend to become progressively more ill-conditioned as the number of trial and test points increase. For cases where it is necessary to employ a large number of points (over a few thousands) the resulting systems are practically unsolvable with the use of standard algorithms.

Several techniques have been proposed to improve the conditioning of the coefficient matrix and the solution accuracy, such as the use of high order interpolation functions, replacement of global solvers by block partitioning, LU decomposition schemes, matrix preconditioners, overlapping and non-overlapping domain decomposition amongst others (see Kansa and Hon (2000)). Although many attempts have been made to resolve these issues, solving practical engineering applications with a global interpolation in RBF meshless collocation methods is still considered prohibitive. In recent years, special attention has been given to the use of local RBF interpolations which are assembled to obtain the entire solution (see Lee et al. (2003) and Shu et al. (2003)).The local strategy results in well-conditioned and banded systems improving the behaviour of this type of meshless methods. In Moroney and Turner (2006), (2007), a local interpolation of the field variable at the cell stencil, based on equation (1), is used to construct the shape functions of the CV-FEM method. The centres of the control volumes belonging to the stencil are used as the corresponding trial and test points of the interpolation.

2 CV-RBF method

For the sake of simplicity, the schematic representations in Figs. 1 to 4 show two-dimensional structured volume elements used to define the collocation centres employed in the interpolation to obtain the local shape functions at the stencils. The proposed method can be directly implemented in two or three dimensional spaces, using structured and unstructured meshes, as it is independent of cell shape and mesh type. The numerical examples reported in this work were obtained with a three dimensional in-house code.

2.1 Mathematical formulation

Consider a steady boundary-value problem which governing equation features a convective term, a diffusion term, a reactive term and a general source

$$L(u) = \frac{\partial}{\partial x_i} D \frac{\partial u}{\partial x_i} - \frac{\partial U_i u}{\partial x_i} + ku = S(x) \quad \Omega \tag{10}$$

$$B(u) = g(x) \quad \partial\Omega \tag{11}$$

$$x \in R^3$$

where u is the unknown field variable, $\vec{U} = (U_1, U_2, U_3)$ is the known convective velocity vector and D and k are the diffusion and reactive coefficients, respectively.

The differential equation integrated over each control volume can then be written as:

$$\int_V \frac{\partial}{\partial x_i} D \frac{\partial u}{\partial x_i} dV - \int_V \frac{\partial U_i u}{\partial x_i} dV + \int_V ku dV = \int_V S(x) dV \tag{12}$$

Applying the divergence theorem, the following equation is obtained

$$\int_S D \frac{\partial u}{\partial x_i} n_i dS - \int_S U_i u n_i dS + kV\overline{u}_p = \overline{S}V \tag{13}$$

where the bar indicates the cell average value operator over a control volume, $\overline{(\bullet)} = 1/V \int_V (\bullet) dV$ and V is the volume of the cell that is considered. If $Nsurf$ is the number of the control volume cell faces, the integral over the control volume surface can be divided into $Nsurf$ sub-integrals

$$\sum_{l=1}^{Nsurf} \int_S D \frac{\partial u}{\partial x_i} n_i dS - \sum_{l=1}^{Nsurf} \int_{S_l} U_i u n_i dS + kV\overline{u}_p = \overline{S}V \tag{14}$$

We now approximate the surface integrals in the above equation with the mid-point rule, by considering the surfaces mean value of the function u and of its gradient to be placed at the mid point of the cell faces. This approximation leads to the following control volume discretisation equation:

$$\sum_{l=1}^{Nsurf} D \left.\frac{\partial u}{\partial x_i}\right|_l n_{li} S_l - \sum_{l=1}^{Nsurf} U_i \, u|_l \, S_l n_{li} + kV\overline{u}_P = \overline{S}V$$

(15)

where n_{li} is the i component of the outward pointing normal to the l^{th} face and S_l the area of the l^{th} surface. To compute the integral approximation in Equation (15) it is necessary to evaluate the function u and its gradient at the mid point of the cell faces. These surface values are given in terms of the cell average values of u in the considered stencil of cells.

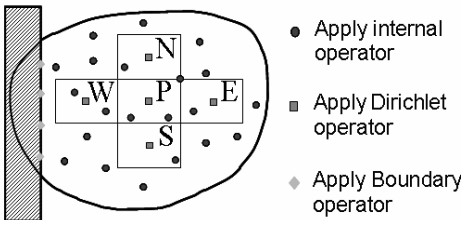

Figure 1: Cell stencil and set of points used by the CV-RBF scheme. Round symbols corresponds to points where the internal (PDE) operator is imposed; square symbols for the Dirichlet operator and diamond symbols for the boundary operator

In Fig. 1, we show a distribution of cells surrounding the control volume under analysis (neighbour cells) plus a set of local scattered data points placed inside or nearby the neighbouring cells. This geometrical configuration is used as the interpolation stencil corresponding to the control volume in consideration. In a stencil close to the boundary, additional points are included at the intersection between the boundary and the stencil, as shown in Fig. 1. Applying a Dirichlet condition at the cell centres the boundary operator (11) at the boundary points and the internal operator (10) at the auxiliary scattered points, we can define a local Hermitian interpolation formula as:

$$\begin{aligned} u(x) = & \sum_{c.centres} \alpha_j \Psi\left(\left\|x-\xi_j\right\|\right) \\ & + \sum_{B.Operator} \alpha_j B_\xi \Psi\left(\left\|x-\xi_j\right\|\right) \\ & + \sum_{I.Operator} \alpha_j L_\xi \Psi\left(\left\|x-\xi_j\right\|\right) + P_{m-1}(x) \end{aligned} \tag{16}$$

By evaluating the different operators on the interpolation formula (16) at the corresponding collocation points, the following algebraic system is obtained for the unknown interpolation coefficients

$$A\alpha = b \tag{17}$$

where

$$\begin{aligned} A &= \begin{pmatrix} [\Psi] & B_\xi[\Psi] & L_\xi[\Psi] & [P_{m-1}] \\ B_x[\Psi] & B_xB_\xi[\Psi] & B_xL_\xi[\Psi] & B_x[P_{m-1}] \\ L_x[\Psi] & L_xB_\xi[\Psi] & L_xL_\xi[\Psi] & L_x[P_{m-1}] \\ \left[P_{m-1}^T\right] & B_x\left[P_{m-1}^T\right] & L_x\left[P_{m-1}^T\right] & [0] \end{pmatrix} \\ b &= \begin{bmatrix} [\overline{u}_{cells}] \\ [g(x)] \\ [S(x)] \\ [0] \end{bmatrix} \end{aligned} \tag{18}$$

with $[\overline{u}_{cells}]^T = (\overline{u}_W, \overline{u}_E, \overline{u}_S, \overline{u}_N, \overline{u}_P)$, as the values of the field variable u at the cells centres. It is important to observe that we have introduced another approximation in formulating the system (17); in fact the value of the function u at the cell centres are taken to be equal to the cell average values.

At this stage it is not possible to determine the coefficients of the Hermitian interpolation, since one part of the right hand side of system (17) is defined by the unknown field variable, i.e. the array $[\overline{u}_{cells}]$ made of the cell-centered average values of the function u. However, the system (17) can be rewritten to express the interpolation coefficients as a function of the unknown $[\overline{u}_{cells}]$ values, as

$$\alpha = A^{-1}b \tag{19}$$

The function u at any point, x_l, inside the stencil, is obtained by substituting the interpolation coefficients given by (19) in (16), as a function of the cells average values $[\overline{u}_{cells}]$, i.e.

$$\begin{aligned} u|_l = & \sum \alpha_j \left(\Psi\left(\left\|x-\xi_j\right\|\right)\right)\Big|_{x=x_l} \\ & + \sum \alpha_j \left(B_\xi \Psi\left(\left\|x-\xi_j\right\|\right)\right)\Big|_{x=x_l} \\ & + \sum \alpha_j \left(L_\xi \Psi\left(\left\|x-\xi_j\right\|\right)\right)\Big|_{x=x_l} \\ & + \left(P_{m-1}(x)\right)\Big|_{x=x_l} \end{aligned} \tag{20}$$

and the corresponding gradient by

$$\left.\frac{\partial u}{\partial x_i}\right|_l = \sum \alpha_j \left(\frac{\partial}{\partial x_i}\Psi\left(\left\|x-\xi_j\right\|\right)\right)\Bigg|_{x=x_l} + \sum \alpha_j \left(\frac{\partial}{\partial x_i}B_\xi\Psi\left(\left\|x-\xi_j\right\|\right)\right)\Bigg|_{x=x_l} + \sum \alpha_j \left(\frac{\partial}{\partial x_i}L_\xi\Psi\left(\left\|x-\xi_j\right\|\right)\right)\Bigg|_{x=x_l} + \left(\frac{\partial}{\partial x_i}P_{m-1}(x)\right)\Bigg|_{x=x_l} \tag{21}$$

Equations (20) and (21) can be written in terms of the vector multiplications

$$u|_l = \overline{C}_{1l}^T\overline{\alpha} \text{ and } \left.\frac{\partial u}{\partial x_i}\right|_l = \overline{C}_{2il}^T\overline{\alpha} \tag{22}$$

where

$$\overline{C}_{1l}^T = \Big(\left[\Psi\left\|x-\xi_j\right\|\right], \left[B_x\Psi\left\|x-\xi_j\right\|\right], \left[L_x\Psi\left\|x-\xi_j\right\|\right], \left[P_{m-1}(x)\right] \Big)\Big|_{x=x_l}$$

and

$$\overline{C}_{2il}^T = \left.\frac{\partial \overline{C}_{1l}^T}{\partial x_i}\right|$$

Finally, choosing the point x_l to be located at the mid point of a face of the integration cell and substituting equation (22) in (15), we obtain

$$\left(\sum_{l=1}^{Nsurf} D\overline{C}_{2il}^T n_{li} S_l - \sum_{l=1}^{Nsurf} U_i n_{li} \overline{C}_{1l}^T S_l\right) \overline{\overline{A}}^{-1}\overline{b} + kV_P\overline{u}_P = \overline{S}V_P \tag{23}$$

Equation (23) is the final CV-RBF formula which couples the field value at the central cell of the stencils, $\overline{u}_P$, with the values at the neighbouring cells centres, $(\overline{u}_W, \overline{u}_E, \overline{u}_S, \overline{u}_N)$. By assembling equation (23) corresponding to all the stencils in the domain a global system of equations for u is obtained. Once the global matrix has been inverted the cell average values of u are found. Knowing the cell average values $[\overline{u}_{cells}]$, considered to be at the control volume centres, the corresponding values of the local interpolation coefficients α are obtained from equation (19). Finally, the solution and its gradient can be reconstructed anywhere inside and in the vicinity of a cell by using equations (20) and (21), see Fig. 2.

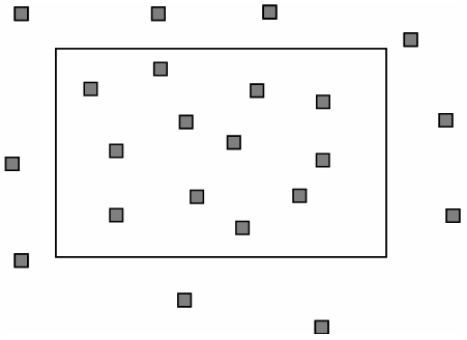

Figure 2: Solution reconstruction points for a single cell

The CV-RBF method developed in this work can be considered as a high order scheme for calculating diffusive fluxes, given the high order accuracy of the RBF derivative approximation (see Madych (1992) and Fornberg and Flyer (2005)). From the viewpoint of the flux calculation, the proposed CV-RBF approach is certainly an improvement on traditional control volume methods. Besides, the requirement of satisfying the governing equation at the local interpolation includes a type of an analytical upwind scheme, given that the resulting interpolation contains the required information about the local velocity field.

In the proposed approach, the extra computational cost to evaluate the local interpolations is of the order $N \times m^3$, where N is the total number of stencils and m is the number of points used for each local interpolation. By keeping the number of interpolation points small (about 10-20), this additional cost is not relevant in comparison with the cost of solving the global system. A possible alternative to reduce this cost is the use of a double collocation at the cell centres in the interpolation algorithm, i.e. requiring that the interpolation simultaneously satisfies the value of the field variable and the governing equation at the cell centres.

It is also important to highlight the flexibility introduced by the meshless nature of the proposed method at local level. In particular this impacts directly on the implementation of the boundary

conditions. Typical constraints of classical control volume schemes, such as the need ghost or dummy cells at the boundaries, are removed by directly imposing the boundary conditions at the solution of the local meshless interpolation problem. In addition boundary conditions can be applied everywhere inside the stencil without being confined to cell faces, opening great opportunities for the investigation of moving boundary problems.

2.2 Stencil configuration

In the previous section, the mathematical formulation for the proposed CV-RBF method has been derived on the basis of a number of stencils equal to the number of cells used to discretise the physical domain. From here on, we call this approach the one-stencil-one-cell configuration. However this is not the only approach that can be considered in the implementation of the proposed new CV approach.

The conservativeness of the numerical scheme is the first condition that needs to be satisfied when choosing the stencil configuration. In the one-stencil-one-cell configuration, as the one sketched in Fig. 3, this property is guaranteed by coupling the neighbouring cells in the local problem formulation. To resolve a particular control volume or cell, the two adjacent cells must be included in the local problem for each face; for example five cells will be considered in Stencil 1 for the lay out shown in Fig 3. The overlapping region formed by cells 1 and 2 guarantees the uniqueness of the flux value for face A when computing the interpolations for stencils, 1 and 2. This is a consequence of the uniqueness of the used Hermitian interpolation at the overlapping region, which is equivalent to the solution of a local boundary value problem.

An alternative to guarantee the conservativeness condition is to form a stencil for each cell face as shown in Fig. 4. We call this the one-stencil-one-face configuration. The face flux is computed only once for every cell face and the cell flux computation takes account of the number of stencils equal to the number of its faces. In Fig. 4 the basic cross stencil needed to calculate the fluxes at

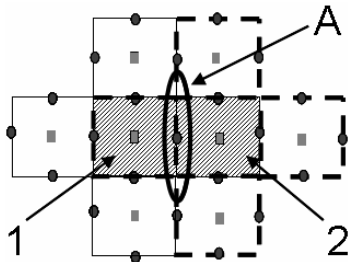

Figure 3: One-stencil-one-cell configuration. Round symbols corresponds to points where the internal (PDE) operator is imposed; square symbols for the Dirichlet operator and diamond symbols for the boundary operator

the faces of cell 1 is split into four simpler problems. This alternative requires the interpolation in those four regions containing the faces of cell 1, but each of them having significant less number of interpolation points in comparison with those used in the one-stencil-one-cell approach.

In terms of computational cost the two configurations described above perform differently. In the one-stencil-one-cell configuration the total number of cells and stencils are the same and equal to N. On the other hand, the one-stencil-one-face alternative requires a larger number of stencils than cells, with the number of stencils equal to βN for N cells, where β changes with the number of dimensions and the type of cell. For the case of 3D problems, the resulting value of β is between three and four. However the impact on the computational cost of the increment in the number of stencils, and consequently the number of local interpolations, for the one-stencil-one-face alternative is somehow balanced by the reduction on the stencil size, as it is evident by comparison of Fig. 4 and Fig. 3.

3 Numerical results

A convergence analysis was carried out for all test cases reported in this section. The results presented for each example correspond to the obtained mesh-independent solutions. A multiquadrics RBF with constant shape parameter was used in the interpolation algorithm. The value of the shape parameter for each case was cho-

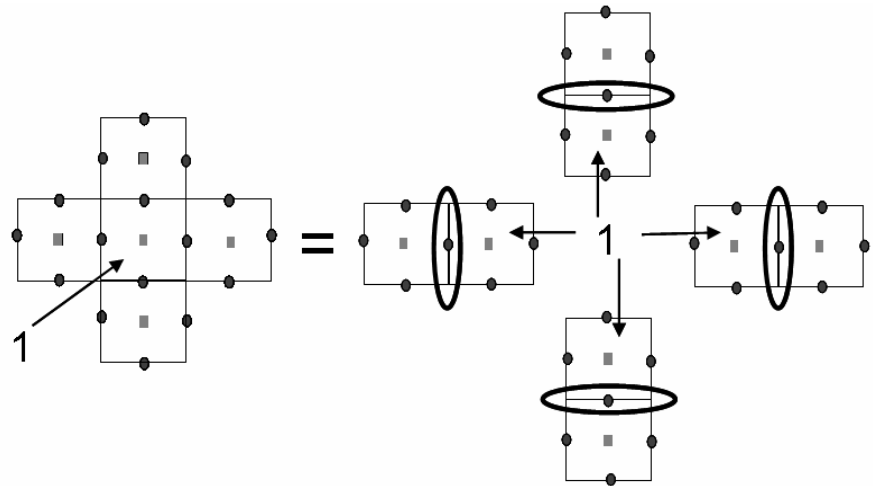

Figure 4: One-stencil-one-face configuration. Round symbols corresponds to points where the internal (PDE) operator is imposed; square symbols for the Dirichlet operator and diamond symbols for the boundary operator

sen experimentally in order to minimize the absolute L2 norm error of the local interpolations. In the computational code used to solve the numerical examples below, both Hermitian (Symmetric) and Kansa (Unsymmetric) methods are implemented to solve the local boundary-value problems. The scheme based on the Hermitian approach is refereed as the CV-HRBF and the one using the Kansa's method as the CV-KRBF. Solutions were obtained with the CV-KRBF and CV-HRBF schemes, as well as with the two different stencil configurations, and their results compared.

3.1 One-dimensional convection-diffusion problem (shock profile)

In this section the steady-state convection-diffusion equation is considered in a channel of dimensions [1.0×0.2×0.2]. The governing equation is given by

$$D\frac{\partial^2\phi}{\partial x_i^2} - \frac{\partial U_i\phi}{\partial x_i} = 0 \tag{24}$$

where D is the diffusion coefficient, U_i the component of the convective velocity in the i direction and ϕ the potential. The following boundary conditions are imposed

$$\phi = 1, \quad x = 0, \quad 0 < y < 0.2, \quad 0 < z < 0.2$$

$$\phi = 2, \quad x = 1, \quad 0 < y < 0.2, \quad 0 < z < 0.2$$

and $\frac{\partial\phi}{\partial n} = 0$ at the remaining walls of the channel. For a one-dimensional convective field, $U_1 = const$ and $U_2 = U_3 = 0$, the above problem has the following analytical solution

$$\phi(x) = 2 - \frac{1-\exp(U_1(x-1))}{1-\exp(-U_1)} \tag{25}$$

In a convection-diffusion problem the parameter that describes the relative influence of the convective and the diffusive components is the Péclet number, $Pe = U_1 L/D$, where U_1 is the longitudinal velocity, L a reference length scale (the channel length in the present case) and D the diffusion coefficient. We have solved the above problem for values of the Péclet number equal to 50, 100, 200 and 400.

In the numerical simulation reported in Fig. 6, a uniform mesh of 41×9×9 points was used to obtain the solution corresponding to the case of a Péclet number of 50, a non uniform mesh of 41×9×9 for the case of a Péclet number of 100 and on a uniform mesh of 81×5×5 points for the cases of Péclet numbers of 200 and 400. A 2D view of the mesh used in each of the above cases at the plane $y = 0.1$ is shown in Fig. 5.

The comparison between the results obtained with the CV-KRBF and CV-HRBF approaches, for the four different Péclet numbers considered, is shown in Fig. 6. For clarity in the presentation, re-

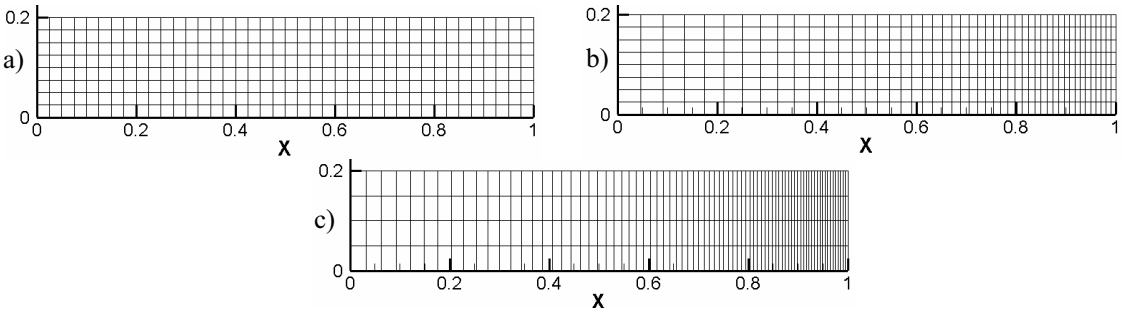

Figure 5: Two-dimensional view at $y = 0.1$ of the three meshes used to solve the diffusive shock: a) uniform with $9\times9\times41$ points, b) non-uniform with $9\times9\times41$ points, c) non uniform with $5\times5\times81$ points

sults are only shown for $x > 0.8$ since the value of the potential is almost constant for $x \leq 0.8$ in the cases considered here. As can be observed from the results in Fig. 6, both CV-RBF approaches are capable of reproducing the analytical solution accurately for the values of the Péclet number considered. However, the CV-KRBF approach always exhibits a larger error at the shock front than that obtained with the CV-HRBF approach. It is important here to address that no systematic algorithm was used to select the shape parameter of the multiquadric function in order to minimize the numerical error in the interpolations. It is possible that the solutions reported in Fig. 6 could be improved by the use of different values of this parameter.

3.2 Axisymmetric Laplace problem

Let us consider the solution of the Laplace equation in a circular cylinder with an internal circular hollow. At the internal and external surfaces a constant value of potential is prescribed. Under these conditions, in cylindrical co-ordinates, the problem is defined by the following axisymmetric equation

$$\frac{1}{r}\frac{d}{dr}\left(r\frac{d\Phi}{dr}\right) = 0 \tag{26}$$

where r is the radial coordinate and ϕ is the potential. By expanding the cylindrical Laplacian operator in equation (26), we obtain the following expression:

$$\frac{d^2\Phi}{dr^2} + \frac{1}{r}\frac{d\Phi}{dr} = 0 \text{ or } \frac{d^2\Phi}{dr^2} + \frac{d}{dr}\left(\frac{1}{r}\Phi\right) + \frac{1}{r^2}\Phi = 0 \tag{27}$$

The analytical solution of this problem is given by

$$\Phi(r) = A + B\ln(r) \tag{28}$$

where

$$A = \left(1 - \frac{\ln(R)}{\ln(R/r_{\min})}\right)\Phi(R) + \frac{\ln(R)}{\ln(R/r_{\min})}\Phi(r_{\min})$$

and

$$B = \left(\frac{\Phi(R) - \Phi(r_{\min})}{\ln(R/r_{\min})}\right)$$

with R and $r_{\min}$ as the external and internal radius, respectively.

Equation (27) can be viewed as a one-dimensional convection-diffusion problem with a variable reaction coefficient, $1/r^2$ and featuring a compressible flow with a negative convective velocity, $-1/r$. In this way, this equation takes the same form of equation (10) with values of $D = 1$, $U_1 = -1/r$, $U_2 = U_3 = 0$, $k = 1/r^2$, $S = 0$ and $\Phi = \Phi(r)$. As can be observed from Equation (28), the analytical solution of this boundary value problem has a singularity when $r = r_{\min} = 0$. The solution of this problem is chosen here to examine the behaviour of the CV-RBF numerical solution in the limit $r_{\min} \to 0$.

The one-dimensional problem defined by equation (27) with boundary conditions $\Phi(R) = 2$ and $\Phi(r_{\min}) = 1$ will be solved here as a 3D problem in a channel defined by the domain $r_{\min} \leq x = r \leq 1$, $0 \leq y \leq 0.2$ and $0 \leq z \leq 0.2$, with zero lateral flux and given constant potential at the inlet and outlet, i.e. $\Phi(x = 1) = 2$ and $\Phi(x = r_{\min}) = 1$.

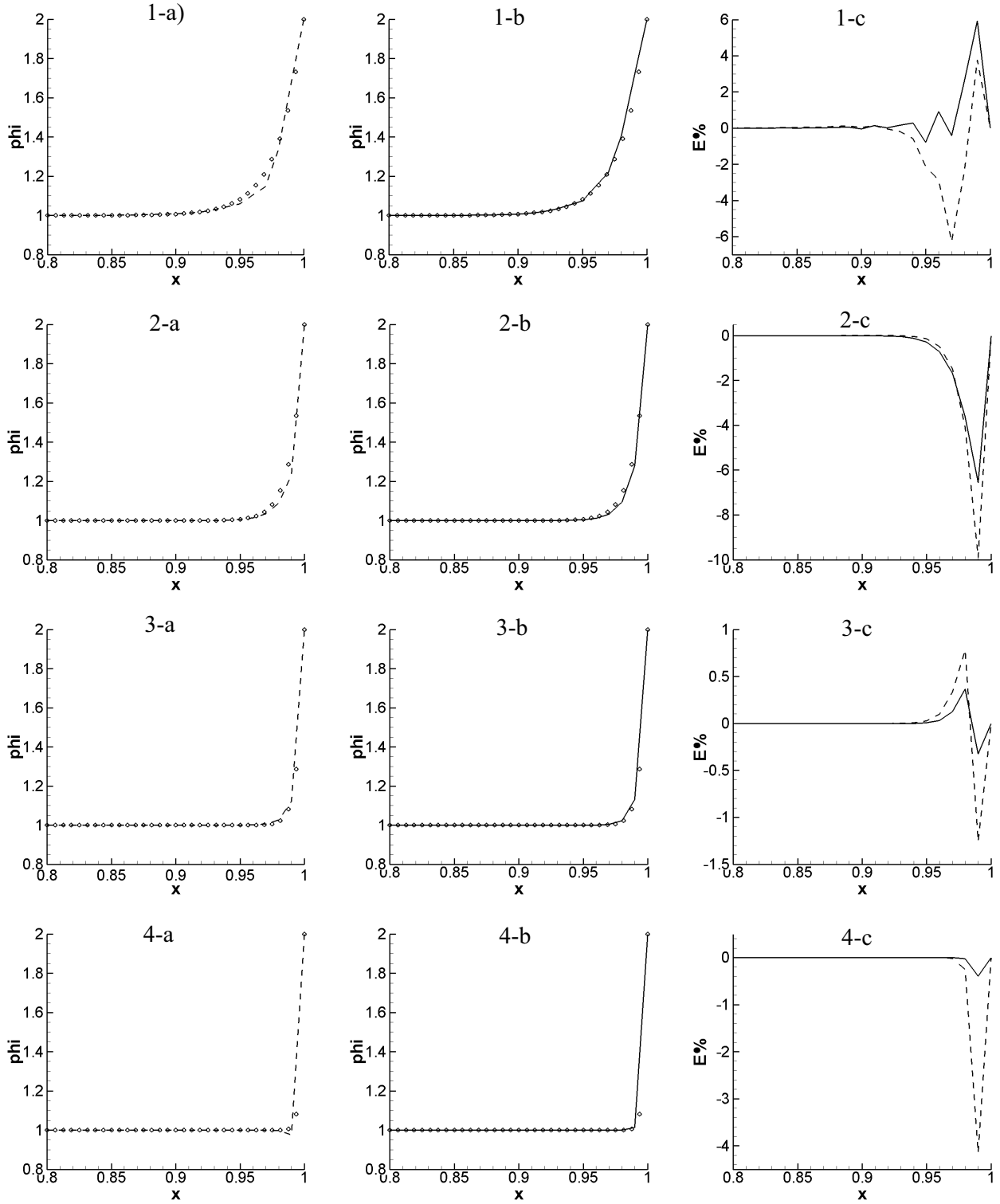

Figure 6: Diffusive shock predictions at four different Pe values: 1) $Pe = 50$, 2) $Pe = 100$, 3) $Pe = 200$, 4) $Pe = 400$; a), CV-KRBF; b), CV-HRBF; c), Relative percentage error. The symbols represent the analytical solutions; the dashed black lines refer to CV-KRBF; the full black lines refer to CV-HRBF

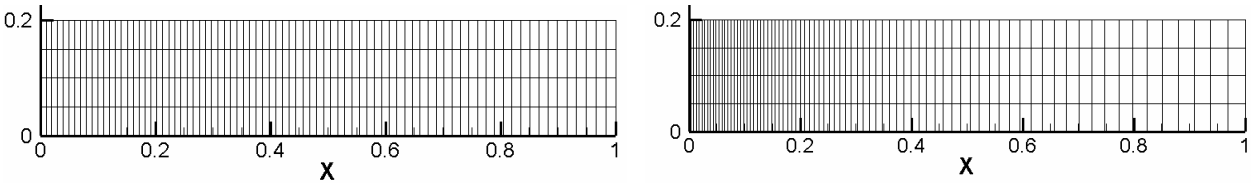

Figure 7: 2D view at y=0.1 of the two meshes used for the computation of Cylindrical Diffusion Problem: a) mesh used for $r_{\min}$ = 0.01, b) mesh used for $r_{\min}$ = 0.003

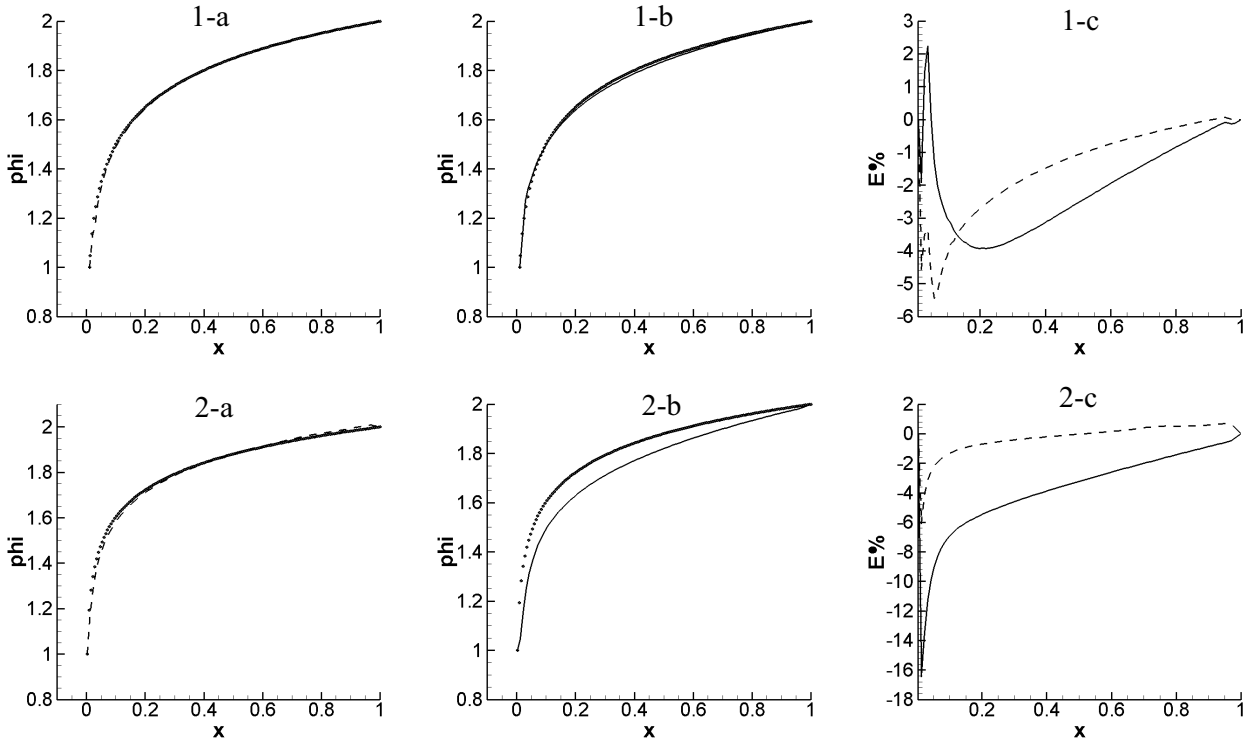

Figure 8: Cylindrical Diffusion Problem: 1) $r_{\min}$=0.01, 2) $r_{\min}$=0.003; a), CV-KRBF; b), CV-HRBF; c), Relative percentage error. The symbols represent the analytical solutions; the dashed black lines refer to CV-KRBF; the full black lines refer to CV-HRBF

Two different values of $r_{\min}$ ($r_{\min}$ = 0.01 and $r_{\min}$ = 0.003) are considered and each of the case is solved using a different mesh. Each mesh consists of 5 points in the y and z directions and 81 points in the x direction. However the mesh used for $r_{\min} = 0.003$ features a larger point density close to the near-singularity, see Fig. 7b.

In Fig. 8 the computed solutions are compared against the analytical solution for both cases. For the case of $r_{\min} = 0.01$, both approaches are able to reproduce the analytical solution with a good degree of accuracy, indicating the ability of the CV-RBF method to handle problems with a strongly varying velocity field and reaction coefficient. However for the case of $r_{\min} = 0.003$, the CV-HRBF method is no longer able to resolve the problem accurately, whereas the CV-KRBF stills matching the analytical solution, see Fig. 8.2a, 8.2b. It appears that the Kansa's scheme interpolation performs better than the Hermitian one in solving this problem. However, as commented before, it must be said at this stage that this is simply an observation valid for the numerical tests carried out here as the shape parameter influence has not yet been fully investigated, and a proper

selection of this parameter could return a different result. The role of varying the shape parameter will be discussed in the next section.

3.3 One-dimensional convection-diffusion problem with a variable velocity

In this section, a one-dimensional convection-diffusion problem with variable velocity is considered. The test case is implemented for a 3D channel of dimension [1.0×0.2×0.2] and the convective velocity is assumed to be a linear function of the longitudinal direction. The governing equation to be solved is equation (24) with

$$U_1 = A + kx$$
$$U_2 = U_3 = 0$$

and $A = \left(\ln \frac{\Phi_{out}}{\Phi_{in}} - \frac{k}{2}\right)$

The above velocity field corresponds to a hypothetical compressible flow with a velocity field changing direction within the domain. Here k is a longitudinal shear stress intensity and Φ_{in} and Φ_{out} are the prescribed inlet and outlet constant values of the potential, respectively (with assigned values of Φ_{in}= 300 and Φ_{out}= 100). In the rest of the domain surfaces symmetry conditions (zero fluxes) are imposed to retain the one-dimensional character of the solution. For simplicity, a unit value was assigned to the diffusion coefficient D.

This problem has a simple analytical solution given by

$$\phi(x) = \Phi_0 \exp\left(\frac{kx^2}{2} + Ax\right) \tag{29}$$

In this case, two diffusive shocks are formed at either ends of the domain, with the central region left relatively "empty". This effect is magnified as the value of k increases. The solution of this problem, presents numerical difficulties as both the large values of ϕ around the shocks and the very small values around the centre of the domain must be predicted accurately. Three different values of k = 40, k = 80 and k= 120, are tested and the computed solutions, using both CV-KRBF and CV-HRBF, are compared against the corresponding analytical solutions in Fig. 9. A uniform mesh of (81×5×5) points is used for k= 40 and a uniform mesh of (101×5×5) points for the other two values of k tested.

The solution is reproduced reasonably well throughout the domain for all the k values tested, with the CV-KRBF still performing slightly better than CV-HRBF, see Fig. 9. It is important to point out that the apparent high relative error obtained at the centre of the domain is due to the dimensionless form used in the definition of the relative error (absolute value of the difference between the numerical and analytical solutions divided by the absolute value of the analytical solution), which results in a division by a very small value of the potential in the centre region of the domain.

It is worth noting that the c-parameter dependency is very strong in this particular example and therefore a comparison between the two methods based on these results alone is inopportune. Changing the c parameter in a bounded range returns solutions which look quite different in particular for large value of k. Fig. 10 exhibits evidence of the effect of the c parameter on the error along a longitudinal section over the entire domain for k =120. This makes clear that the shape factor c is a data-dependent parameter and does not only depend on the geometry and the physics of the problem alone.

3.4 Three-dimensional convection-diffusion problem with variable velocity

In this section the CV-RBF is validated in a three-dimensional convection-diffusion problem with a variable velocity field. The equation solved is Equation (24) with the components of the convective velocity field given by

$$U_1 = ax$$
$$U_2 = -by$$
$$U_3 = c$$

corresponding to a linear shear compressible flow with a constant density and a constant mass source term $\rho(a-b)$. The potential function given by the expression (30) is a general solution of convection-diffusion equation with the above pa-

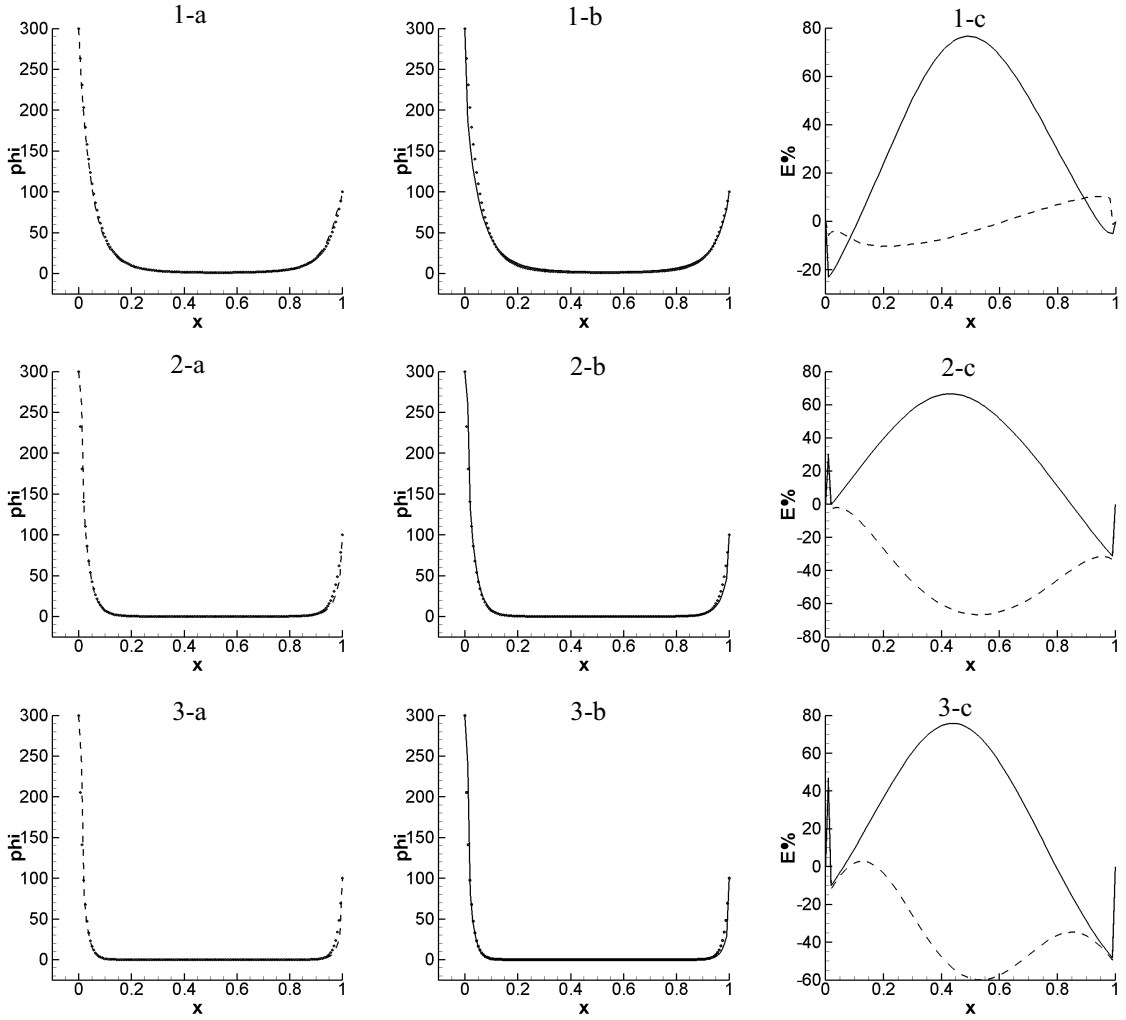

Figure 9: Variable velocity with reaction term problem, at three different k values: 1) k=40, 2) k=80, 3) k=120; a), CV-KRBF; b), CV-HRBF; c), Relative percentage error. The symbols represent the analytical solutions; the dashed black lines refer to CV-KRBF; the full black lines refer to CV-HRBF

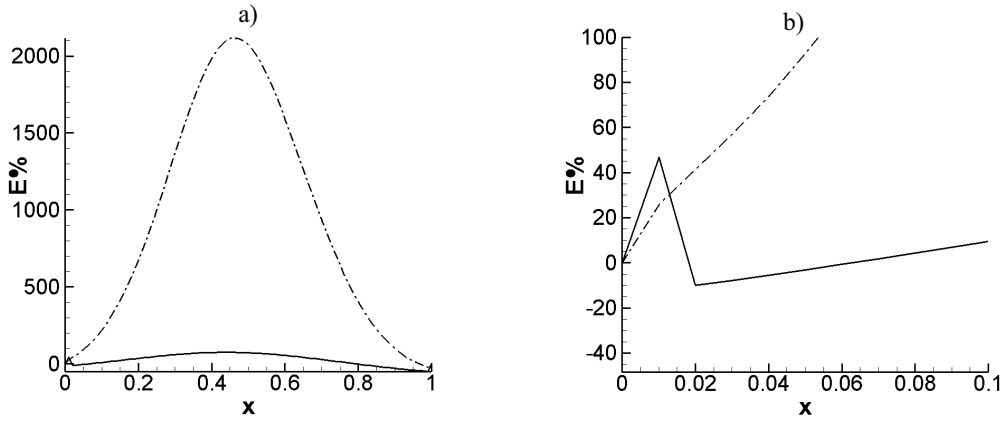

Figure 10: Variable velocity with reaction term problem, CV-HRBF, k=120, influence of the c parameter on the solution. Full line, simulation using c=0.001; Dot dashed line, simulation using c=0.01; a), full scale plot; b) zoom on the bottom left corner of the full scale plot

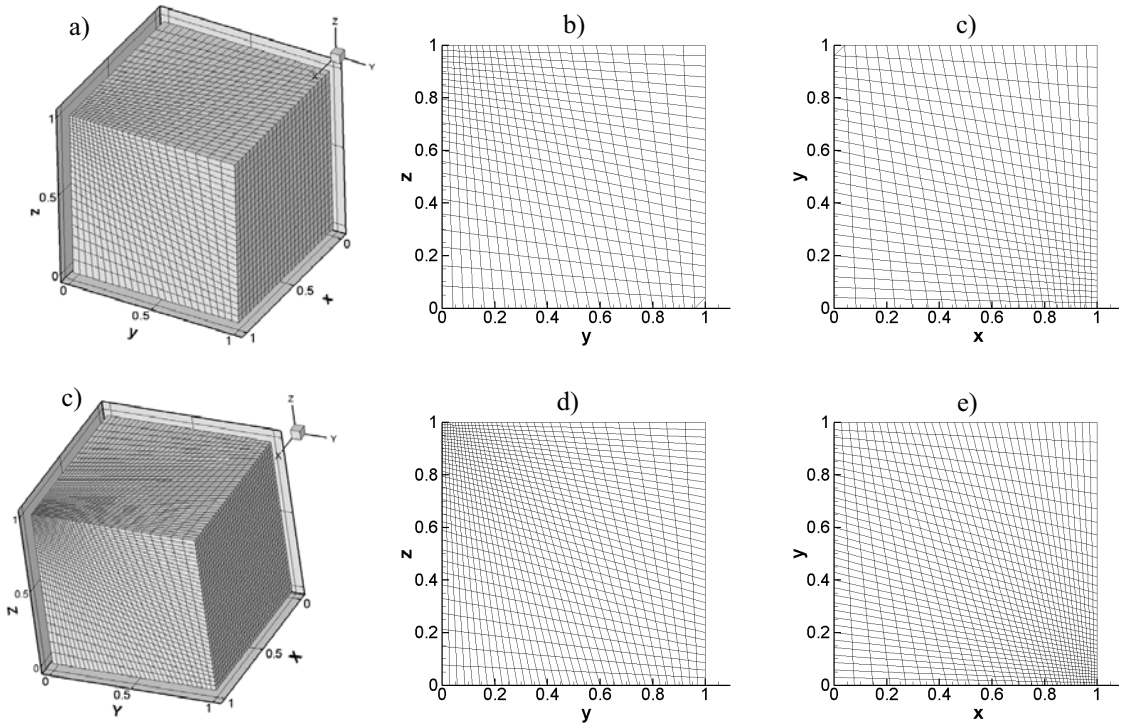

Figure 11: Mesh used to solve the three-dimensional convection-diffusion problem: a) coarse mesh, three-dimensional view; b) coarse mesh, view at x=0.96; b) coarse mesh, view at z=0.96; c) fine mesh three-dimensional view; d) fine mesh, view at x=0.97; e) fine mesh, view at z=0.97

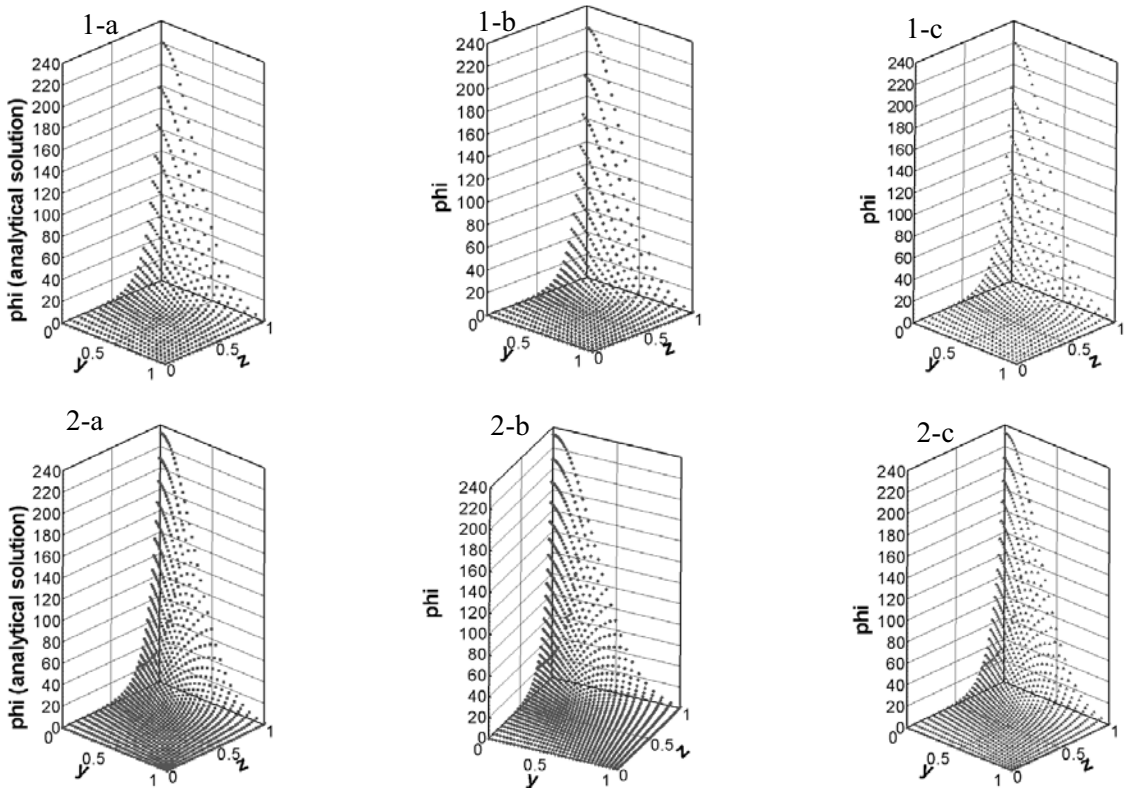

Figure 12: Solution 3D plots: 1) x=0.96 for the coarse mesh, 2) x=0.97 for the fine mesh. a) - analytical solution; b) one-stencil-one-cell solution, c) one-stencil-one-face solution

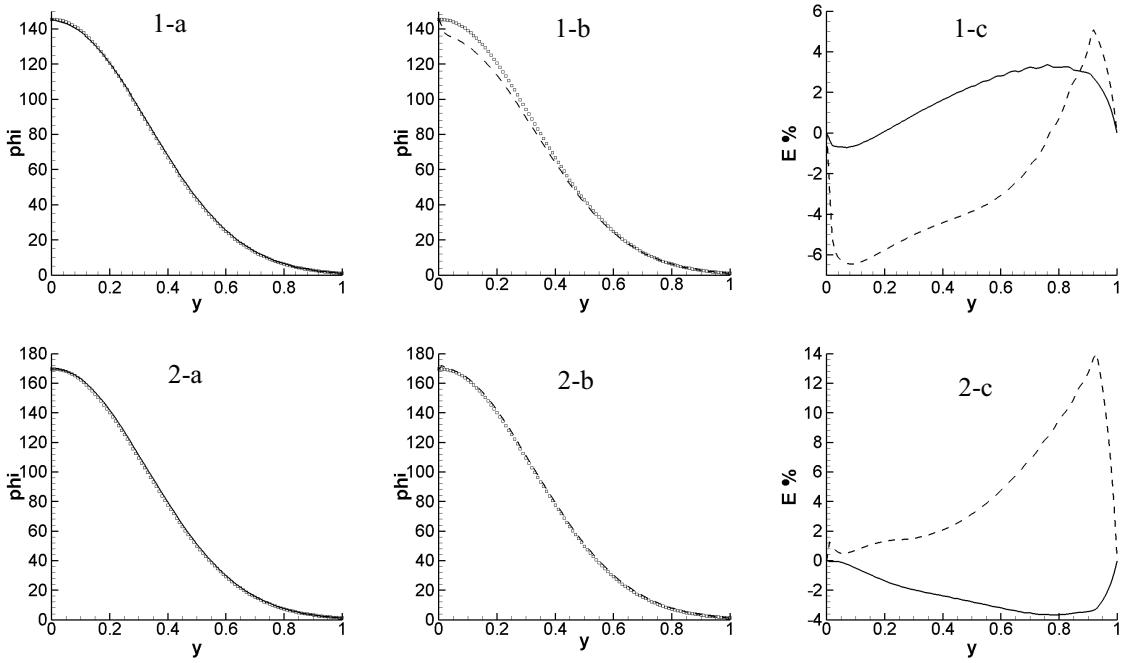

Figure 13: Profiles extracted close to the shock: 1) at x=0.96, z=0.96, $0 \leq y \geq 1$ for the coarse mesh; 2) at x=0.97, z=0.97, $0 \leq y \geq 1$ for the fine mesh; a), one-stencil-one-cell configuration b), one-stencil-one-face configuration; c), Relative percentage error. The symbols represent the analytical solutions; the dashed lines refer to one-stencil-one-face configuration; the full lines refer to one-stencil-one-cell configuration

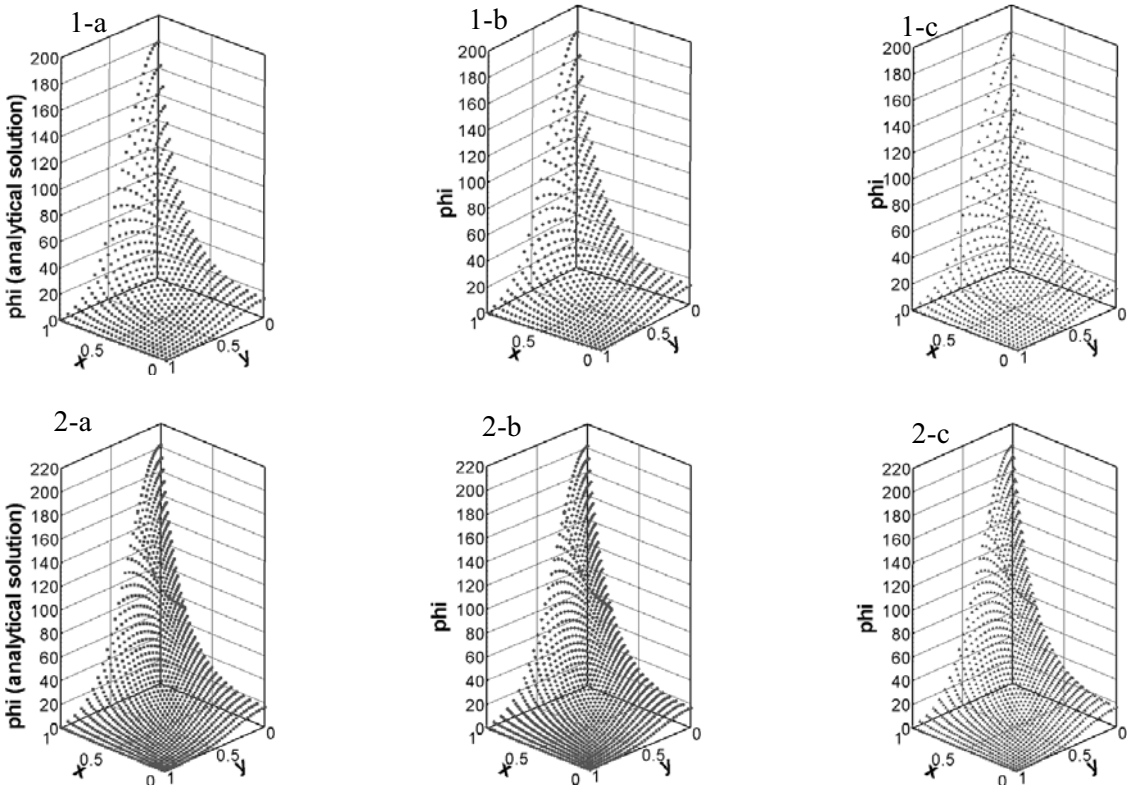

Figure 14: Solution 3D plots: 1) z=0.96 for the coarse mesh, 2) z=0.97 for the fine mesh. a) - analytical solution; b) one-stencil-one-cell solution, c) one-stencil-one-face solution

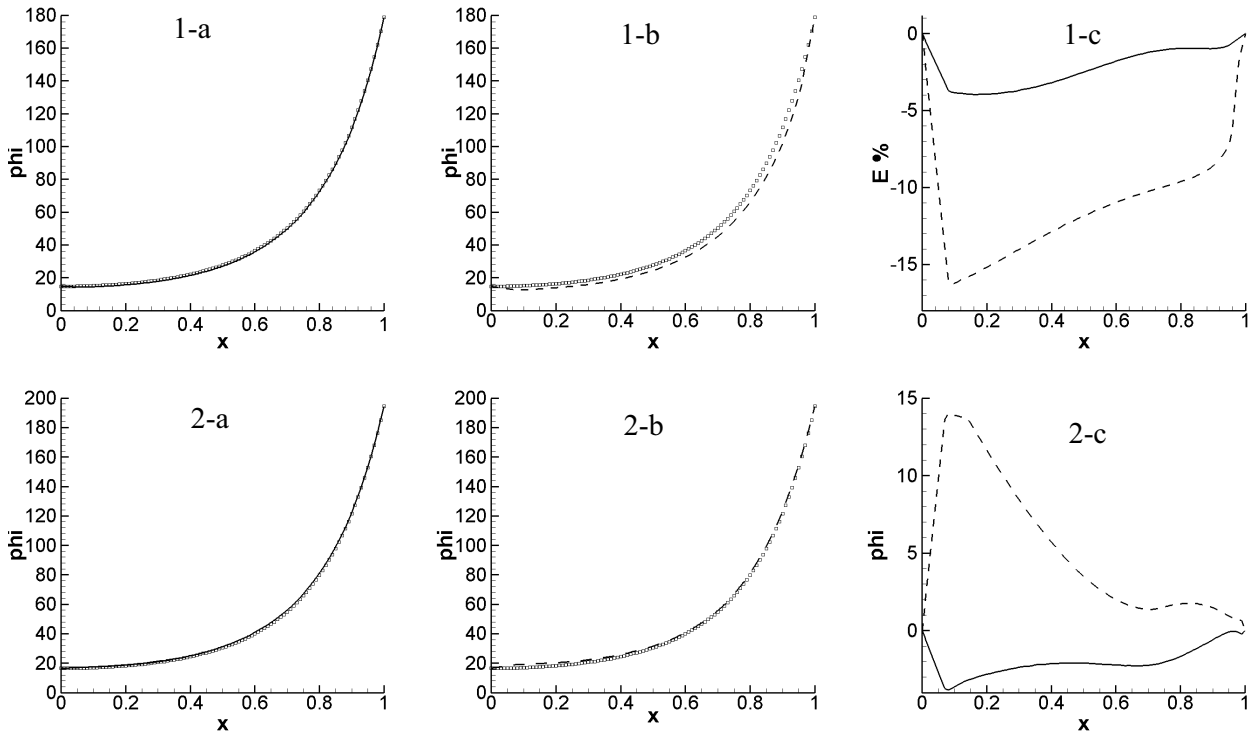

Figure 15: Profiles extracted close to the shock: 1) at y=0.04, z=0.96, $0 \leq x \geq 1$ for the coarse mesh; 2) at y=0.028, z=0.97, $0 \leq x \geq 1$ for the fine mesh; a), one-stencil-one-cell configuration b), one-stencil-one-face configuration; c), Relative percentage error. The symbols represent the analytical solutions; the dashed lines refer to one-stencil-one-face configuration; the full lines refer to one-stencil-one-cell configuration

rameters

$$\phi = A \exp\left[\frac{1}{2D}\left(ax^2 - by^2 + 2cz\right)\right] \tag{30}$$

where are A is an arbitrary constant.

The proposed CV-RBF method was used to solve a 3D convection-diffusion problem, solution of equation (24) with the above convective velocity field, in a cubic domain of dimension $[1\times1\times1]$ using the potential function given in (30) to prescribe Dirichlet boundary conditions on the six cube faces, for values of A= 0.001, $D = 0.1$, $a = 0.5$ and $b = 1$. The solution of this problem shows a strong convection towards one of the domain corner where a smooth shock is formed.

For this three dimensional problem no remarkable differences have been noticed between the solutions obtained with the CV-KRBF and CV-HRBF methods whereas the two stencil configurations introduced in Section 3 lead to different outcomes and exhibit different sensitivities to the mesh.

In this example two different meshes were tested, a coarser mesh with $26\times26\times26$ points, corresponding to 15,625 cells, and a finer one with $36\times36\times36$ points, corresponding to 42,875 cells. Both computational grids presents a non-uniform points distribution with a refinement in the region of the expected shock, see Fig. 11. To assess the accuracy of the method and the behaviour of the two proposed stencil configurations, the numerical results are presented in two slices close to regions of high gradients. The first one is a plane of constant x value, at x=0.96 for the coarse mesh and x=0.97 for the fine mesh, and the second one a plane of constant z value, at z=0.96 for the coarse mesh and z=0.97 for the fine mesh. For these two slices three-dimensional solution plots are reported in Figs. 12 and 14 for both meshes and both stencil configurations. The analytical solution is also plotted on these planes for comparison purposes. Corresponding detailed profiles are plotted in two dimensions in Figs. 13 and 15 for

clarity, where the analytical solution is also presented for comparison purposes.

The one-stencil-one-face approach fails in the shock region when the coarse mesh is used. It undershoots the exact solution and is not able to predict the correct concave shape. This problem does not come across in the case of the one-stencil-one-cell configuration where the single cell stencil employed is larger and guarantees a local interpolation that better describes the solution in all directions. The drawback reported for the one-stencil-one-face configuration improves with the use of the finer mesh but its solution still having lower accuracy in comparison with the solution obtained with the one-stencil-one-cell configuration using the same finer mesh. It is also worth noticing that the slices and the profiles analysed for the finer mesh are closer to the shock front than the sections considered for the coarse mesh.

4 Conclusion

A new numerical scheme has been formulated with the main objective to exploit the possible advantages of coupling the meshless RBF collocation approach and the CV methods. The proposed method can be considered meshless only at the local level of the interpolation stencils, where a boundary value problem is solved for every cell to define the cell shape functions from which the evaluation of the flux across the cell faces is obtained. This circumstance increases the accuracy of the flux computation and at the same time provides an analytical upwind scheme since the local interpolation satisfies the PDE operator and therefore contains information about the physics of the problem. Two different cell stencil configurations have been proposed both guaranteeing the conservativeness of the scheme which preserves the main advantage of the CV method. The new numerical approach has been tested in series of one- and three-dimensional convection-diffusion problems, which show the capabilities of method in predicting phenomena characterized by high Péclet numbers.

Acknowledgement: This research was sponsored by the European Commission GABARDINE project (Contract no: 518118), sixth framework program, priority 1.1.6.3 (Global change and Ecosystems). The authors would like to thank the anonymous reviewers for their helpful comments and suggestions.

References

Abgrall R. (1994): On essentially Non-Oscillatory Schemes on Unstructured Meshes: Analysis and Implementation, *Journal of Computational Physics*, **114**, 45-98.

Baliga B.R.; Patankar S.V. (1980): A new finite-element formulation for convection-diffusion problems, *Numerical Heat Transfer*, **3**, 393-409.

Ben Salah M.; Askri F.; Ben Nasrallah S. (2005): Unstructured Control-Volume Finite-Element Method for Radiative Heat Transfer in a Complex 2-D Geometry, *Numerical Heat Transfer, Part B: Fundamentals,* **48**(5), 459-475.

Brown D. (2005): On Approximate Cardinal Preconditioning Methods for Solving PDEs with Radial Basis Functions, *Engineering Analysis with Boundary Elements,* **29**(4), 343-353.

Date A.W. (2005): Solution of transport equations on unstructured meshes with cell-centered colocated variables. Part I: Discretization, *International Journal of Heat and Mass Transfer,* **48**, 1117-1127.

Dubal M.R.; Olivera S.R.; Matzner R.A. (1993): *Approaches to Numerical Relativity*. Cambridge UK, Cambridge University Press.

Dumbser M.; Kaser M. (2007): Arbitrary high order non-oscillatory finite volume schemes on unstructured meshes for linear hyperbolic systems, *Journal of Computational Physics,* **211**, 693-723.

Fasshauer G.E. (1997). Solving Partial Differential Equations by Collocation with Radial Basis functions, *Proceedings of Chamonix,* Chamonix, Vanderbilt University Press, Nashville, USA.

Fedoseyev A.I.; Friedmann M.J.; Kansa E.J. (2002): Improved multiquadratic method for elliptic partial differential equation via PDE collocation on the boundary, *Computers & Mathematics with Applications,* **43**, 439-455.

Fornberg B.; Flyer N. (2005): Accuracy of radial basis function interpolation and derivative approximations on 1-D infinite grids, *Advances in Computational Mathematics,* **23**(1), 5-20.

Franke C.; Schaback R. (1998): Convergence order estimates of meshless collocation methods using radial basis functions, *Advances in Computational Mathematics,* **8**, 381-399.

Grissa H.; Askri F.; Ben Salah M.; Ben Nasrallah S. (2007): Three-dimensional radiative transfer modeling using the control volume finite element method, *Journal of Quantitative Spectroscopy and Radiative Transfer,* **105**(3), 388-404.

Hon Y.C.; Mao X.Z. (1998): An efficient numerical scheme for Burgers' equation, *Applied Mathematics and Computation,* **95**(1), 37-50.

Jayantha P.A.; Turner I.W. (2003): A second order finite volume technique for simulating transport in anisotropic media, *International Journal of Numerical Methods for Heat & Fluid Flow,* **13**(1), 31-56.

Jayantha P.A.; Turner I.W. (2005): A Second Order Control-Volume Finite-Element Least-Squares Strategy For Simulating Diffusion In Strongly Anisotropic Media, *Journal of Computational Mathematics,* **23**(1), 1-16.

Jumarhon B.; Amini S.; Chen K. (2000): The Hermite collocation method using radial basis functions, *Engineering Analysis with Boundary Elements,* **24**(7-8), 607-611.

Kansa E.J.; Hon Y.C. (2000): Circumventing the Ill-Conditioning Problem with Multiquadric Radial Basis Functions: Applications to Elliptic Partial Differential Equations, *Computers & Mathematics with applications,* **39**, 123-137.

La Rocca A.; Hernandez Rosales A.; Power H. (2005): Radial basis function Hermite collocation approach for the solution of time dependent convection-diffusion problems, *Engineering Analysis with Boundary Elements,* **29**(4), 359-370.

Lee C.; Liu X.; Fan S. (2003): Local multiquadric approximation for solving boundary value problems, *Computational Mechanics,* **30**, 396-409.

Ling L.; Opfer R.; Schaback R. (2006): Results on meshless collocation techniques, *Engineering Analysis with Boundary Elements,* **30**(4), 247-253.

Liu F.; Turner I.W.; Anh V. (2002): An unstructured mesh finite volume method for modelling saltwater intrusion into costal aquifers, *Journal of Applied Mathematics & Computing,* **9**, 391-407.

Madych W.R. (1992): Miscellaneous error bounds for multiquadric and related interpolators, *Computers & Mathematics with applications,* **24**(12), 121-138.

Madych W.R.; Nelson S.A. (1990): Multivariate Interpolation and Conditionally Positive Definite Functions. II, *Mathematics of Computation,* **54**, 211-230.

Manzini G.; Putti M. (2007): Mesh locking effects in the finite volume solution of 2-D anisotropic diffusion equations, *Journal of Computational Physics,* **220**, 751-771.

May-Duy A.N.; Tran-Cong T.; Tanner R.I. (2006): New High-order Time-kernel BIEM for the Burgers Equation, *CMES: Computer Modeling in Engineering and Sciences,* **16**, 177-186.

Micchelli C. A. (1986): Interpolation of scattered data: Distance matrices and conditionally positive definite functions, *Constructive Approximation,* **2**(1), 11-22.

Moroney T.J.; Turner I.W. (2006): A finite volume method based on radial basis functions for two-dimensional nonlinear diffusion equations, *Applied Mathematical Modelling,* **30**(10), 1118-1133.

Moroney T.J.; Turner I.W. (2007): A three-dimensional finite volume method based on radial basis functions for the accurate computational modelling of nonlinear diffusion equations, *Journal of Computational Physics,* **225**(2), 1409-1426.

Nguyen-Van H.; Mai Duy N.; Tran-Cong T. (2007): A simple and accurate four-node quadrilateral element using stabilized nodal integration for laminated plates, *CMC: Computers, Materials and Continua,* **6**, 159-176.

Ollivier-Gooch C.; Van Altena M. (2002): A

High-Order-Accurate Unstructured Mesh Finite-Volume Scheme for the Advection-Diffusion Equation, *Journal of Computational Physics,* **181**, 729-752

Powell M.J.D. (1994): The uniform convergence of thin plate spline interpolation in two dimensions, *Numerische Mathematik,* **68**, 107-128.

Power H.; Barraco V. (2002): A comparison analysis between unsymmetric and symmetric radial basis function collocation methods for the numerical solution of partial differential equations, *Computers and Mathematics with Application,* **43**, 551-583.

Rousse D.R. (2000): Numerical predictions of two-dimensional conduction, convection, and radiation heat transfer. I. Formulation, *International Journal of Thermal Sciences,* **39**(3), 315-331.

Schaback R. (1995). Multivariate interpolation and approximation by translates of a basis function, *Approximation Theory VIII*, World Scientific Publishing Co, London, UK.

Shu C.; Ding H.; Yeo K. (2003): Local radial basis function-based differential quadrature method and its application to solve two-dimensional incompressible Navier-Stokes equations, *Computer methods in applied mechanics and engineering,* **192**, 941-954.

Sladek V.; Sladek J.; Tanaka M. (2005): Local Integral Equations and two Meshless Polynomial Interpolations with Application to Potential Problems in Non-homogeneous Media, *CMES: Computer Modeling in Engineering and Sciences,* **7**(1), 69-84.

Truscott S.L.; Turner I.W. (2004): An Investigation of the Accuracy of the Control-Volume Finite-Element Method Based on Triangular Prismatic Elements For Simulating Diffusion in Anisotropic Media, *Numerical Heat Transfer, Part B: Fundamentals,* **46**, 243-268.

Turner I.W.; Ferguson W.J. (1995): An unstructured mesh cell-centered control volume method for simulating heat and mass transfer in porous media: Application to softwood drying, Part I: The isotropic model, *Applied Mathematical Modelling,* **19**(11), 654-667.

Versteeg H.K.; Malalasekera W. (2007). *The Finite Volume Method*, Pearson Education Limited, Boston, USA.

Wen P.H.; Hon Y.C. (2007): Geometrically Nonlinear Analysis of Reissner-Mindlin Plate by Meshless Computation, *CMES: Computer Modeling in Engineering and Sciences,* **21**, 177-192.

Wright G.; Fornberg B. (2006): Scattered node compact finite difference-type formulas generated from radial basis functions, *Journal of Computational Physics,* **212**(1), 99-123.

Wu Z. (1992): Hermite-Birkhoff interpolation of scattered data by radial basis functions, *Approximation Theory,* **8**(2), 1-11.

Wu Z. (1998). Solving PDEs with radial basis functions and the error estimation; , *Advances in Computational Mathematics*, , Lectures in Pure and Applied Mathematics, Eds. Z. Chen, Y. Li, C.A. Micchelli, Y. Xu & M. Dekker, Taylor & Francis, CRC Press, London, UK.

Young D.L.; Chen C.S.; Wong T.K. (2005): Solution of Maxwell's Equations Using the MQ Method, *CMC: Computers, Materials and Continua,* **2**, 267-276.